Synthesis and Characterization of Chromate Conversion Coatings on GALVALUME and Galvanized Steel Substrates

M.A. DOMÍNGUEZ-CRESPO, E. ONOFRE-BUSTAMANTE, A.M. TORRES-HUERTA, F.J. RODRÍGUEZ-GÓMEZ, S.E. RODIL, and A. FLORES-VELA

The morphology, composition, and corrosion performance of chromate conversion coatings (CCCs) formed on GALVALUME (Fe-Al-Zn) and galvanized steel (Fe-Zn) samples have been studied, and different immersion times (0, 10, 30, and 60 seconds) have been compared. The coated surfaces were analyzed using light microscopy, X-ray diffraction (XRD), scanning electron microscopy (SEM), and electrochemical measurements in a NaCl solution (3 wt pct). The electrochemical measurements were carried out using the polarization resistance, Tafel, and ac impedance methods. A nonuniform growth of the CCCs having a porous morphology and cracks that appear extended to the base metal was observed. The XRD patterns show that the coatings mainly consist of CrO_3, Cr_2O_3, and traces of $Cr_2O_7^{-2}$. The electrochemical results show that GALVALUME presents a better behavior than that of the galvanized steel alloys at each dipping time. The SEM micrographs show that the galvanized steel treatments resulted in the formation of a more uniform film, but their protection barrier broke down faster than that of the GALVALUME samples in contact with the aggressive media. The samples that underwent the lowest degree of dissolution were those with a dipping time of 30 seconds. The difference in the corrosion protection given by the two substrate types could be attributed to the structural properties, grain size, composition, and roughness, which affect oxygen diffusion.

DOI: 10.1007/s11661-009-9856-7

I. INTRODUCTION

CHROMATE conversion coatings (CCCs) have traditionally been employed to prevent the corrosion process in several metallic components and to improve the adhesion of paints, lacquers, and organic components.[1,2] Although these coatings are highly effective, chromium (VI), which is used in the conversion treatment, is a carcinogenic agent.[3,4] Nowadays, as a consequence of the environmental and health risks associated with the use of such coatings, they are being restricted.

M.A. DOMÍNGUEZ-CRESPO, Professor, formerly with the Universidad Nacional Autónoma de México, Edificio D Facultad de Química, Departamento de Metalurgia. Ciudad Universitaria, C.P. 04510 México D.F., México, is with the Instituto Politécnico Nacional, Grupo de Ingeniería en Procesamiento de Materiales CICATA-IPN, Unidad Altamira. Km 14.5, Carretera Tampico-Puerto Industrial Altamira. C.P. 89600 Altamira, Tamps. México. Contact e-mail: mdominguezc@ipn.mx E. ONOFRE-BUSTAMANTE and F.J. RODRÍGUEZ-GÓMEZ, Professors, are with the Universidad Nacional Autónoma de México, Edificio D Facultad de Química, Departamento de Metalurgia. Ciudad Universitaria. A.M. TORRES-HUERTA and A. FLORES-VELA, Professors, are with the Instituto Politécnico Nacional, Grupo de Ingeniería en Procesamiento de Materiales CICATA-IPN, Unidad Altamira. Km 14.5, Carretera Tampico-Puerto Industrial Altamira. C.P. 89600. Altamira, Tamps. México. S.E. RODIL, Professor, is with the Universidad Nacional Autónoma de México, Instituto de Investigación en Materiales, Circuito Exterior s/n, Ciudad Universitaria. Del. Coyoacán, C.P. 04510 México D.F., México.

Manuscript submitted February 18, 2008.
Article published online June 11, 2009

Several alternatives have been investigated in recent years, which have led to the development of other nontoxic coating processes with comparable adhesion properties and corrosion protection. For example, zinc, manganese, and iron compounds have been employed together with fluorides,[5] and more recently, new types of conversion pretreatments formed by immersion in solutions containing cerium chloride, phosphates, or other rare earth metal chlorides, such as yttrium and lanthanum, have been studied.[6–9] However, processes with similar performances to that of Cr (VI) have not yet been achieved.

Cr (VI) provides an exceptionally good corrosion resistance, which depends upon the base metal, treatment, and film thickness. The protection is due to both the corrosion inhibition effect of the hexavalent chromium contained in the film and the physical barrier by the film itself. Even scratched or abraded films retain a great deal of their protective value, because the hexavalent chromium content is slowly leachable in contact with the moisture, providing a self-healing effect.[10–12]

The mechanism by which conventional CCCs inhibit the corrosion of metals is not yet fully understood, although a large number of studies have been performed and some insight has been obtained.[13–15] In order to understand the process and the effect of some parameters such as temperature, pH, immersion time, and substrate, a detailed characterization is required.

Some techniques, such as scanning electron microscopy (SEM), transmission electron microscopy

(TEM),[16,17] X-ray photoelectron spectroscopy,[18] Auger electron spectroscopy,[19] and, recently, spectroscopic ellipsometry[20] as a nondestructive method, have been found to be very useful tools for studying the chemical composition and the element depth concentration profiles of CCCs. This information can also be useful in understanding the corrosion protection or the coating adhesion enhancement offered by these chemical treatments. These characterization techniques are usually combined with some nondestructive electrochemical techniques such as resistance polarization and electrochemical impedance spectroscopy.

The aim of this work is to obtain a better understanding of the corrosion resistance provided by the CCC treatments by studying the effect of different immersion times and the role played by the composition and microstructure of the substrate. The corrosion performance of treated galvanized steel (Fe-Zn) and GALVALUME* (Fe-Al-Zn) surfaces immersed 10, 30, and 60 seconds in a Chronak solution (200 g/L $K_2Cr_2O_7$ and 10 g L^{-1} H_2SO_4) was studied.[21] The electrochemical measurements were carried out in a NaCl solution (3 wt pct), and their response was correlated with the morphology and elemental compositions.

*GALVALUME is a trademark of BIEC, International Inc., Vancouver, WA.

II. EXPERIMENTAL

A. *Substrate Characterization*

All the tests were carried out at least three times with commercially available galvanized steel and GALVALUME sheets, and the average of the results was considered as the final report. In order to better understand the effect of these two different types of substrates on the corrosion behavior of the CCCs, we performed a previous characterization of the substrates. Continuous immersion tests were conducted using a NaCl solution (3 wt pct) during 4 weeks at room temperature.

B. *CCC Processes*

In this study, commercial Fe-Zn and Fe-Al-Zn sheets, 2.25 cm^2 and a thickness of 2 mm, were employed. Before immersion, the metallic samples were degreased using acetone followed by ethanol, and then they were finally dried in air. The CCCs were obtained by dipping the commercial samples in the conventional Chronak solution (200 g L^{-1} $K_2Cr_2O_7$ and 10 g L^{-1} H_2SO_4) at room temperature and pH = 1.1,[21] for 10, 30, and 60 seconds. The coatings were then rinsed, air dried, and aged at room temperature for 24 hours before any further handling or analysis.

C. *Surface Characterization of CCCs*

The structural characterization was carried out by XRD using a Siemens 5000 diffractometer, operated at 35 kV and 25 mA with a curve graphite crystal monochromator and broad focus cupper source. The samples were scanned at a speed of 2 deg min^{-1} between 15 and 100 deg.

Morphological aspects of the substrates and the conversion layers were also studied by light and scanning electron microscopes (EDS) JEOL** JSM-35C equipped with an EDS Voyager Tracor Northern Spectrometer.† The chemical composition was also scanned by EDS analysis.

**JEOL is a trademark of Japan Electron Optics Ltd., Tokyo, Japan.

†Voyager Tracor Northern Spectrometer is a trademark of Noran Instruments Inc., Middleton, WI now Thermo Electron Coporation, Camas, WA.

D. *Electrochemical Measurements*

The electrochemical measurements consisted of open circuit potential monitoring (E_{ocp}), polarization resistance (*Rp*), Tafel, and ac impedance. The samples were tested in a NaCl aqueous solution (3 wt pct) at room temperature. A standard three-electrode setup was used. The electrochemical cell consisted of an acrylic rectangular box (60 × 80 × 100 mm), and the exposed area of the sample was 0.785 cm^2. The specimens were introduced by moderate pressure against an O-ring, avoiding localized damage of the chromate layer.

The counterelectrode was a large-area graphite bar, and the reference electrode was a saturated calomel electrode (SCE, 0.2415 V *vs* SHE). The electrochemical curves were generated by an ac Gill‡ potentiostatic-galvanostatic equipment connected to a personal computer.

‡Gill is a trademark of ACM instruments, Cumbria, UK.

The polarization resistance measurements were conducted by scanning the potential from OCP to ±30 mV, at 10 mV min^{-1} scan rate. During all the electrochemical measurements, each sample was maintained at the open circuit potential until the potential was stabilized. The Tafel polarization curves were measured from cathodic to anodic area. The scans were started at −250 mV *vs* SCE with a sweep rate of 1 mV s^{-1}.

The coating resistance was determined by electrochemical impedance spectroscopy (EIS) in the frequency region going from 10,000 to 0.01 Hz, ten frequency points per decade with amplitude of 10 mV root-mean-square (rms) at room temperature. In order to prevent any influence from previous polarization, each measurement was taken from a new area of the sample.

E. *Pull-Off Test*

For the adhesion strength, the substrates were painted with a commercial polyurethane varnish using a micrometric film aluminum applicator. All the specimens showed a dry film thickness between 80 and 100 μm, which was measured with a surface profiler (digital coating thickness gage, C.C. Elcometer[§] 106 series), according to the ASTM D-4541 standard. The specimens for each test were glued onto an aluminum stud of 21-mm diameter with epoxy resin, followed by a drying process at room temperature during 24 hours.

[§]C.C. Elcometer is a trademark of Elcometer, Inc., Rochester Hills, MI.

III. RESULTS AND DISCUSSION

The major steps of the coating process are pretreatment of the substrate surfaces prior to coating, deposition of the conversion coating, and treatment of the coated surfaces after deposition. In this work, some of these steps will be discussed in terms of the effect that they have on the immersion time, composition of the substrate, morphology, or performance of the chromate conversion coatings.

A. *Substrate Characterization*

Figure 1 shows the corrosion rate *vs* time for GALVALUME and galvanized steel. The corrosion rate calculations were estimated from weight loss data using the following equation:[22,23]

$$MPY = \frac{534W}{DAT} \quad [1]$$

where W is the weight loss in milligrams, D is the density in grams per cubic centimeter, A the area in square inches, T the time in hours, and MPY is the corrosion rate in mils (1 mil = 0.001 in.) of the penetration per year.

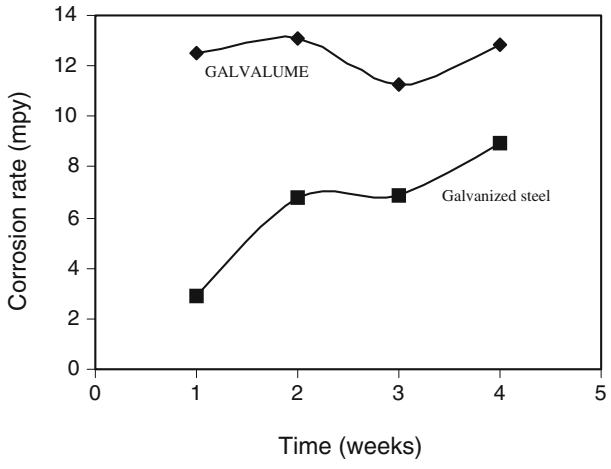

Fig. 1—Effect of the substrate on the corrosion rate in continuous immersion using a 3 wt pct NaCl aqueous solution.

By comparing the results concerning the GALVALUME and galvanized steel samples, it can be observed that the GALVALUME corrosion rate is higher than that of the galvanized steel specimens. Figure 1 also shows an almost constant corrosion rate for GALVALUME with an average near 12.4 *MPY*. On the other hand, at the beginning, lower corrosion rate values were observed for galvanized steel; however, the weight loss was drastically increased in these samples with the immersion time. After the first week, an average near 7.6 *MPY* was observed. The stabilization of the corrosion rate could correspond to either a uniform corrosion regime or surface topology modifications or both. This behavior can also be correlated with larger current values and porosity on the substrate surface.

The characterization of the substrate suggests that the corrosion rate and the passive film formed in GALVALUME during the gravimetric tests are more stable than the galvanized steel samples. This probably causes a localized corrosion or pitting in the galvanized steel specimens even though the corrosion resistance of the Fe-Al-Zn samples seems to be more affected by the presence of Cl^- ions. The surface damages on Fe-Zn and Fe-Al-Zn caused by the corrosion process can be related to the discrete events, which are governed by statistical laws describing the metal-electrolyte system, and the systems undertake successive state modifications through a minimum energy path.[24]

Figure 2 shows the SEM micrographs of the substrates after 4 weeks in continuous immersion in a NaCl solution. GALVALUME exhibited a typical corrosion process of the Al-Zn coatings (Figure 2(a)), which can be observed as small crystals. The composition on the substrate surface could correspond to Al_2O_3, ZnO, and some iron oxides (Table I). For the galvanized steel specimens, the observed morphology was more uniform than that for GALVALUME, and the surface analysis could be correlated to ZnO and iron oxides (Figure 2(b)). The thickness of the Al-Zn and Zn coatings on the Fe matrix was also determined by SEM (Figure 3). An average film thickness of 22 and 14 μm can be observed from these micrographs for GALVALUME and galvanized steel, respectively. It is well known that the proper selection of the coating thickness requires the knowledge of the corrosiveness of the environment in which the material will be used and matches the desired material life and cost. However, because the corrosion resistance strongly depends on the microstructural features of the coating, it is more important to have the right microstructure than a thick coating. It has been found that in order to achieve the desired microstructure during the production, the coating thickness must not be too thin (>7 μm).[25–29] Then, we assume that, in our case, the variation of the corrosion performance of the substrate is not greatly affected by the variation of the coating thickness, and the results can be comparable to each other. In the reported literature on galvanized steel or GALVALUME corrosion, the performance has been mainly described on the basis of Zn or Zn-Al layer corrosion without mentioning the role of the intermetallic

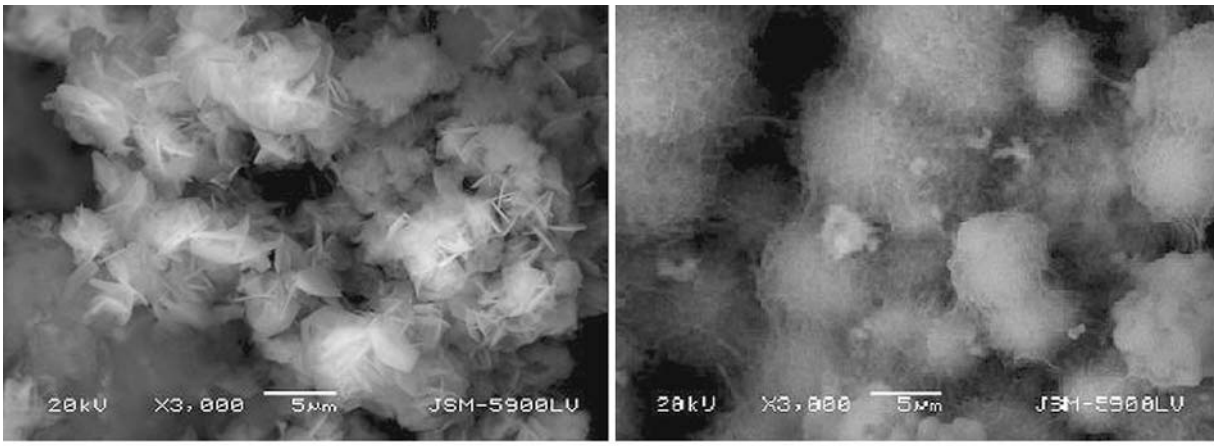

Fig. 2—SEM micrographs of the substrate after 4 weeks in continuous immersion in a 3 wt pct NaCl aqueous solution: (*a*) GALVALUME and (*b*) galvanized steel.

Table I. EDS Analysis for the Elements and Normalized Results for the Surface Substrates

Sample	Element	Wt Pct
GALVALUME	Al	35.45
	Fe	4.31
	Zn	20.28
	O	39.96
Galvanized steel	Fe	1.26
	Zn	70.77
	O	27.97

layers that are formed during the process.[25,26] However, from the quantitative results in this study, it could be seen that the galvanized steel coating layer is composed of three phases: η phase (Zn), ζ phase (Fe-Zn_x), and steel. The microstructure of the GALVALUME coating has four principal phases: one phase is the primary aluminum-rich dendritic phase that begins to grow initially during the solidification, an interdendritic zinc-rich region that forms when the zinc concentration in the solidifying liquid reaches a high level, an intermetallic (Fe-Al-Si-Zn) phase, and steel. These phases can generate different textural characteristics (preferred crystallographic orientation), although the texture of the films strongly depends on external factors such as cooling rate, gradient, surface condition of the steel substrate during the coating solidification process, and bath chemical composition (Fe-Al-Zn or Fe-Zn).[29–31] Concerning the coating corrosion resistance and post-treatments, these also depend on the zinc layer chemical composition and are affected by the crystallographic orientation. When a metal is exposed to a corrosive

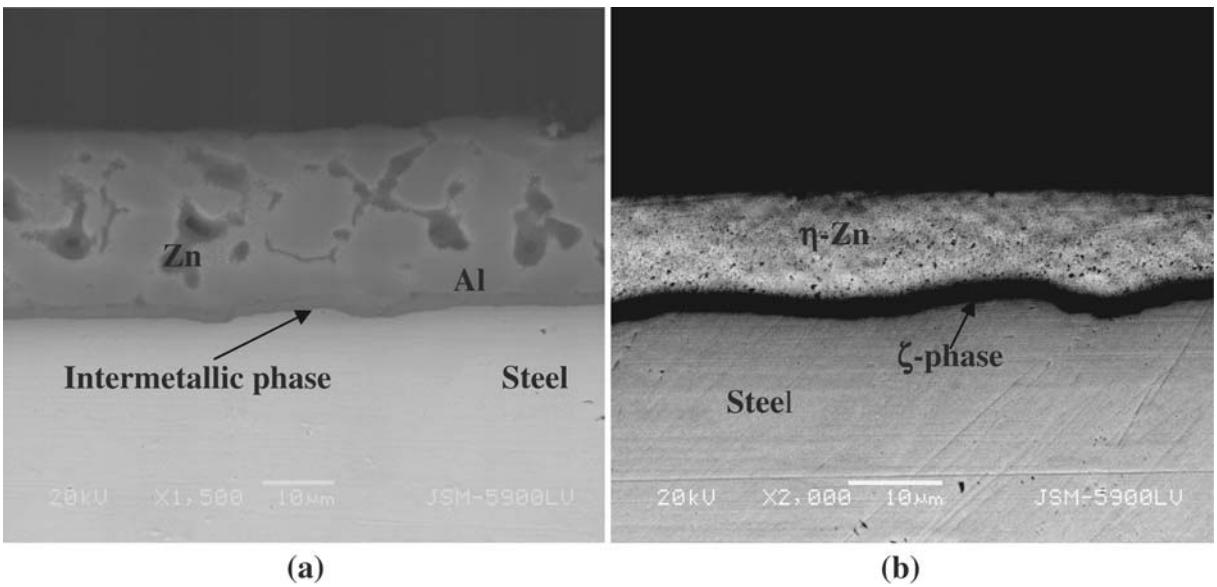

Fig. 3—SEM cross sections showing the thickness in (*a*) GALVALUME and (*b*) galvanized steel.

environment, the corrosion resistance of each grain varies because of the difference in the binding energy of the atoms between the crystallographic planes. According to Scully, the total energy involved in the breaking of the bonds and the subsequent dissolution of atoms is higher for the crystallographic planes, which have a higher number of neighboring atoms. Thus, the close-packed planes, or low-index planes, are known to be more resistant to dissolution because of the higher binding energy of the surface atoms.[30]

In this way, the largest corrosion rate measured for GALVALUME could be due to the parabolic corrosion rate that can be displayed in most environments, which is attributable to the dendritic structure.[27,28] When the coating is exposed to the aggressive media, the zinc-rich areas are corroded first. Since these areas are located in a labyrinth of interdendritic region in the coating, the corrosion products tend to fill the interdendritic interstices and the corrosion rate stabilizes or decreases, which is in contrast with the typical linear behavior of galvanized steel.

B. *Microstructural Characterization of CCCs*

Figure 4 shows the optical morphology of the bare and chemically treated specimens at room temperature. It can be seen that in the GALVALUME substrates, the grains have regular sizes. It should be noted that this morphology is the general morphology after the CCCs were applied onto samples (Figures 4(a) and (c)). The aforementioned suggests that the conversion coatings grew without preferential direction. The CCCs deposited on the galvanized steel are thin plates; their edges lie in one direction on each grain, and there is a change in the morphology from one grain to another grain (Figures 4(b) and (d)). In general, the samples could correspond to the layered thin hexagonal platelets with a thin lamellar type reported elsewhere.[29]

In order to properly understand the role of the substrate on the film formation, SEM images for chromate coatings on Fe-Al-Zn and Fe-Zn alloys with dipping times of 10, 30, and 60 seconds were analyzed (Figures 5 and 6).

Figures 5(a) through (d) show that the particle shape forming the film on the GALVALUME specimens is irregular, which causes certain porosity and nonhomogeneity on them; therefore, two zones can be distinguished. The first region consists of dispersed islands, and the second area includes a lower thickness film that covers some zones of the alloy; in these zones, the substrate microstructure is visible because the layer is very thin. The film thickness and size of the particles

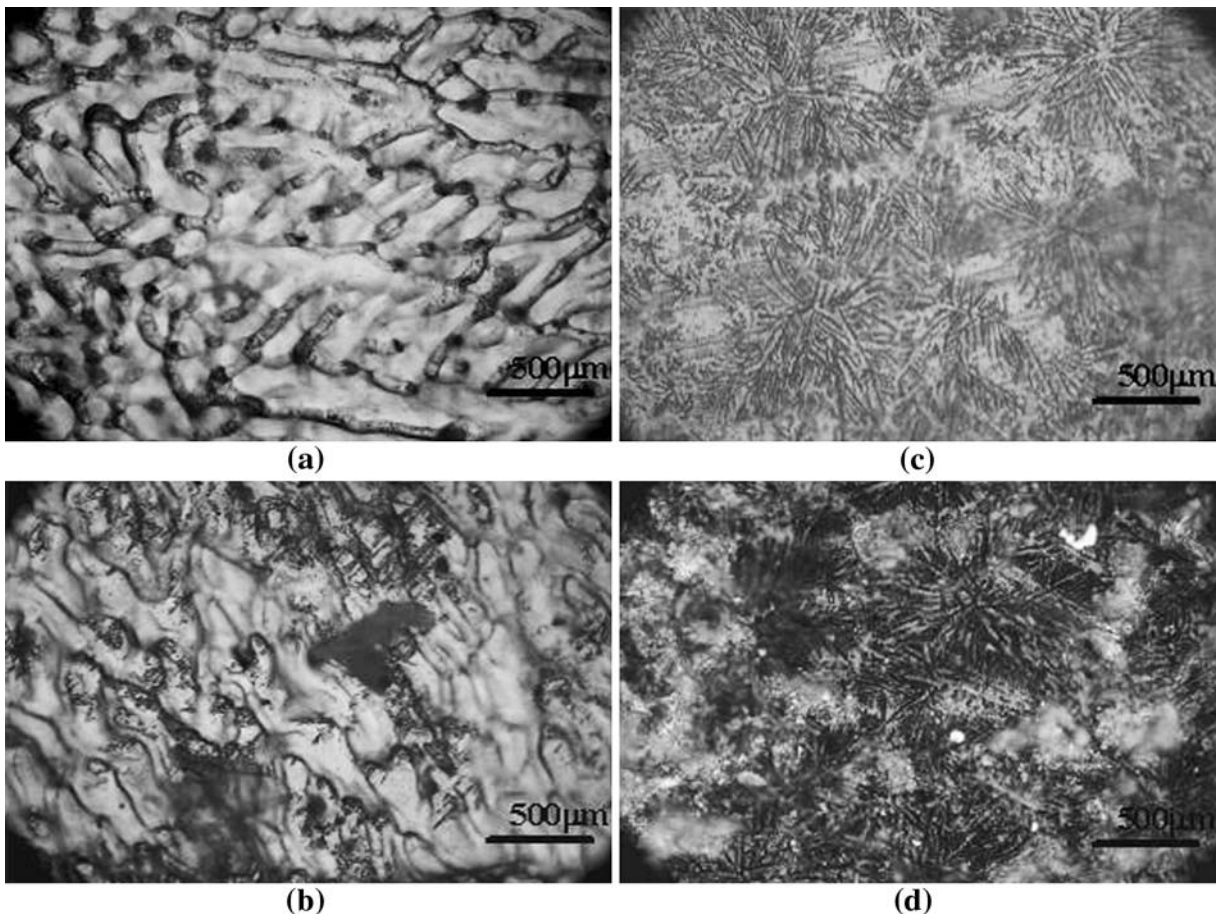

Fig. 4—Light microscopy images for GALVALUME (*a*) before and (*b*) after 60 s of treatment, and galvanized steel (*c*) before and (*d*) after 60 s of treatment.

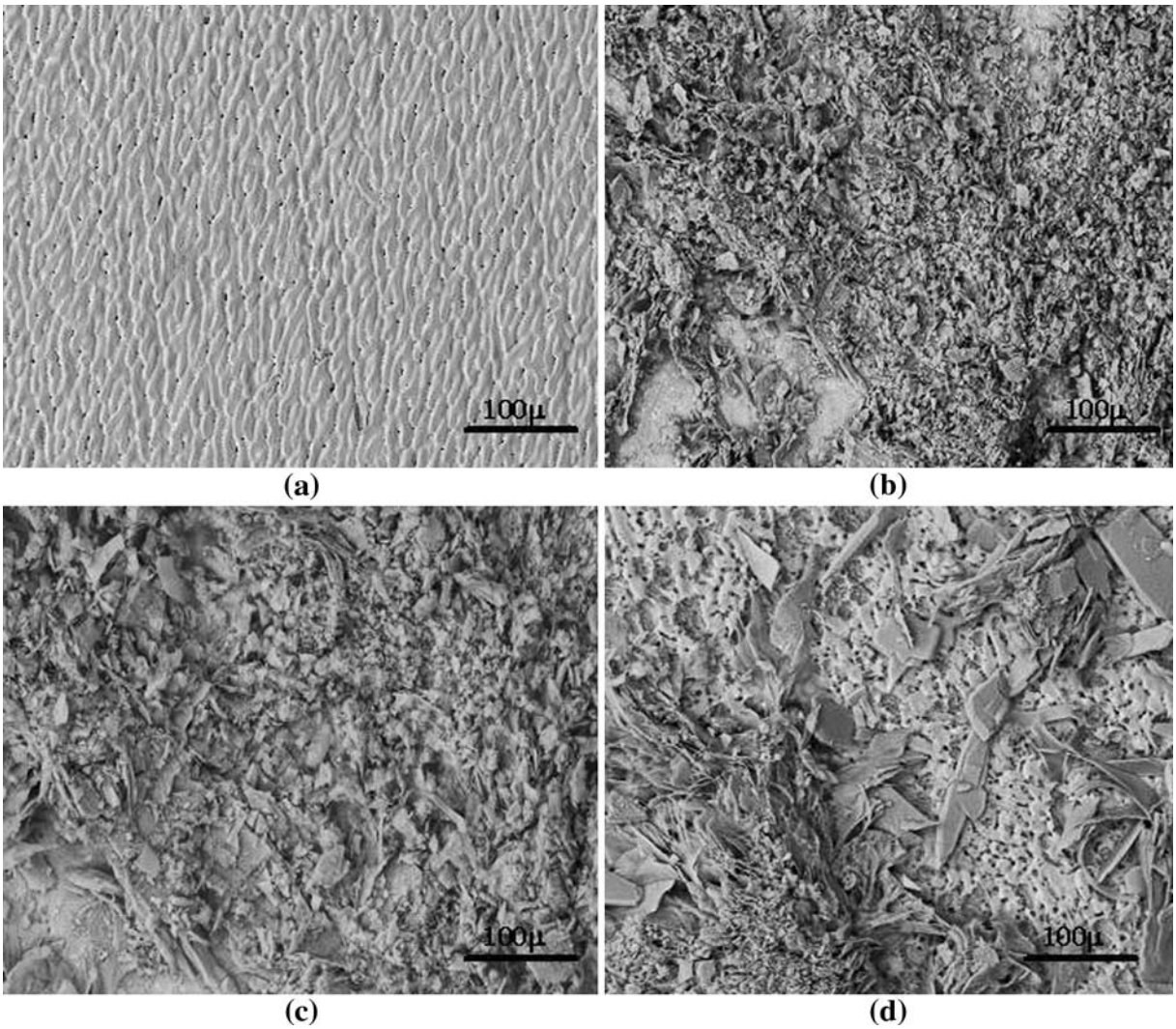

Fig. 5—SEM results of GALVALUME conversion layers obtained in chromate baths at (*a*) 0 s, (*b*)10 s, (*c*) 30 s, and (*d*) 60 s of immersion time.

with irregular shape as well as the roughness and porosity of the film are increased with the immersion time. The Fe-Al-Zn alloys with dipping times of 10 and 30 seconds almost covered the substrate surface unlike that obtained with 60 seconds. This suggests that times longer than 30 seconds can cause a slight attack on the substrate surface, generating a higher porosity, which could lead to an increase in the film degradation in aggressive media.

Figures 6(a) through (d) show the SEM images of the treated Fe-Zn alloys at different immersion times. After 10 seconds, it was observed that the thin film is not well formed, but it is uniform and spreads to cover the substrate surface. For the samples with dipping times longer than 10 seconds, the crack length per unit area and the crack width are increased. These cracks look like platelets with sharp and well-defined edges. In the preparation of the coating, it is known that the coating has a gel-like structure before drying, but during the stage of drying, the coating would shrink and the shrinkage process would result in the formation of microcracks with ''dried riverbed'' patterns.[32]

Table II presents the EDS analysis of the GALVALUME and galvanized steel samples obtained after the chemical conversion coatings. These studies were done in areas with and without cracks. The table shows that the microanalysis of the CCCs in the crack tips was different from that in the uncracked region. However, the amount of chromium is higher as the immersion time is increased. During the EDS analysis, the Al, Zn, and Fe contents were high, and this was due to the effect of the Fe-Al-Zn and Fe-Zn alloys. Although the SEM/EDS results are just an approximation and further studies will be required to determine the CCCs composition, their tendency might have an influence on the electrochemical behavior or the adhesion of the paint coatings, which will be discussed later on.

The obtained results match the light microscopy measurements, which indicate that the formation and growth of chromate conversion coatings on GALVALUME were not uniform on the surface, whereas for galvanized steel, the film was more homogenous. The CCC growth was strongly affected by the substrate surface. As a particular case, the coating formed on

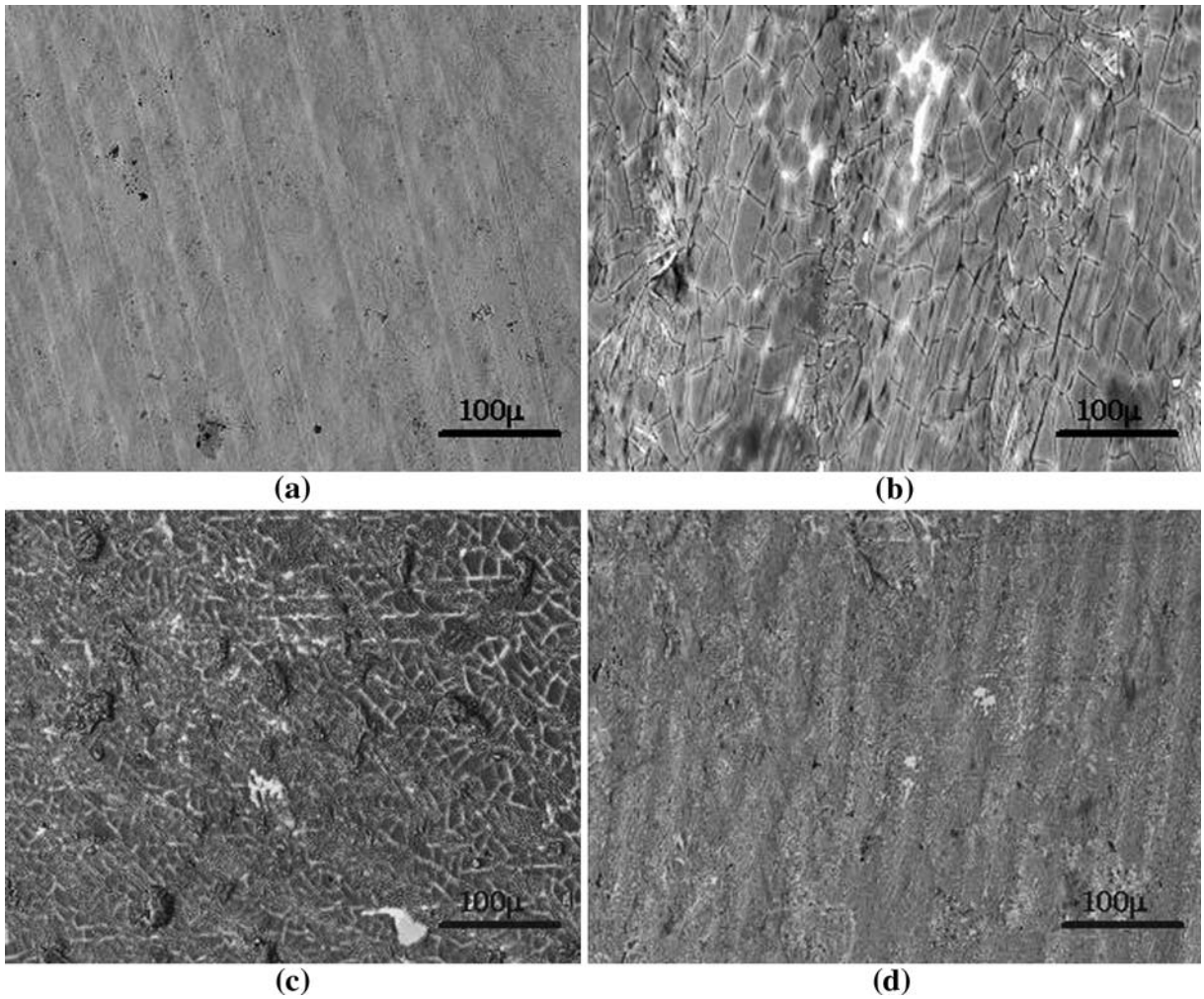

Fig. 6—SEM backscattered results of galvanized steel conversion layers obtained in chromate baths at (*a*) 0 s, (*b*) 10 s, (*c*) 30 s, and (*d*) 60 s of immersion time.

Fe-Al-Zn consisted of small crystals randomly distributed on the surface, and whose size was larger than those obtained on the Fe-Zn matrix. These results are in good agreement with Lunder *et al.*,[33] who analyzed some aluminum alloys and obtained poor coverage at grain boundaries when CCCs were applied as treatment. Their deposited chromium oxide was also characterized by a porous morphology with cracks that apparently extend down to the metal base. Our SEM images also show microcrack formation on the CCCs on galvanized steel, probably as a consequence of tensile stress inside the coating. The results mentioned previously point out that the morphology and the composition of the substrate play an important role during the growth of the chemical conversion coating. As it is known, corrosion in this kind of chromate coatings starts and propagates along cracks within the coatings, and these cracks are attributable to the tensile stress during the growth of the film; as a consequence, they are increased with chromate thickness, which could explain the SEM observations at longer immersion times.[34,35] Then, an increase in the number of microcracks, porosity, and thickness can appear in the CCCs on Fe-Al-Zn and Fe-Zn alloys when the dipping time is longer than 10 seconds. These results are also in agreement with the results obtained by Zhang *et al.*,[36] who additionally suggested that for Fe-Zn alloys, the chromate layer displays cathodic inhibition.

The ellipsometric analysis for the treated chromium conversion coating specimens was done to calculate the thickness of the CCCs by fitting the acquired spectroscopic ellipsometry spectra using a two-layer optical model previously used to model the optical properties of CCCs on aluminum[20,37] selecting a wavelength range of 400 to 1700 nm; however, unfortunately, the characteristics of the film (pale yellow and thickness) caused a high absorption light, so it was not possible to determine the thickness with good accuracy, as previously reported by Zhang.[36] However, from the SEM measurements, it was clear that the treatment thickness increases with the immersion time. From these micrographs, the semi-quantitative measurements of the chromate film thicknesses ranged from 900 to 1500 nm, which are higher than those reported in the literature and could explain the high light dispersion.[36,37]

Table II. EDS Analysis for the Elements and Normalized Results after CCCs

10 s				
	GALVALUME		Galvanized Steel	
Element	Reaction Area (At. Pct)	Crack Area (At. Pct)	Reaction Area (At. Pct)	Crack Area (At. Pct)
C	24.79	23.52	35.64	37.46
O	20.33	9.40	30.89	7.75
Al	27.42	46.63	0.92	1.17
K	7.67	1.38	7.83	1.93
Cr	7.03	1.17	7.53	1.60
Fe	—	—	0.66	—
Zn	12.55	17.91	16.52	50.09
Total	100.00	100.00	100.00	100.00

30 s				
	GALVALUME		Galvanized Steel	
Element	Reaction Area (At. Pct)	Crack Area (At. Pct)	Reaction Area (At. Pct)	Crack Area (At. Pct)
C	18.66	22.65	27.18	28.78
O	15.27	6.89	27.13	10.64
Al	27.17	45.33	0.73	1.39
K	10.80	1.97	8.68	3.17
Cr	10.21	1.92	8.22	2.42
Fe	—	—	—	—
Zn	17.89	21.24	28.06	53.61
Total	100.00	100.00	100.00	100.00

60 s				
	GALVALUME		Galvanized Steel	
Element	Reaction Area (At. Pct)	Crack Area (At. Pct)	Reaction Area (At. Pct)	Crack Area (At. Pct)
C	16.28	23.15	28.20	31.17
O	35.01	7.84	20.08	9.62
Al	17.38	39.55	1.13	2.21
K	6.07	5.29	10.03	2.03
Cr	16.23	4.52	9.71	2.59
Fe	—	—	—	—
Zn	9.03	19.65	30.86	52.38
Total	100.00	100.00	100.00	100.00

The chemical composition of the samples was analyzed by XRD. Figures 7(a) and (b) show the typical diffraction patterns of GALVALUME and galvanized steel sheets. The characteristic XRD spectra have been compared with previous works, and the coatings were confirmed.[32,38] Fe-Al-Zn substrates before the chromate coatings display peaks of hexagonal zinc and cubic aluminum, while the Fe-Zn samples only present hexagonal zinc. After 10, 30, and 60 seconds of dipping time in chromate baths, CrO_3, $Cr_2O_7^{-2}$, and Cr_2O_3 were detected in both kinds of substrates, and their intensities increased with the immersion time, although for the Fe-Zn samples, the chromium (III) and (VI) species displayed a poorer intensity and broadening than those observed in GALVALUME, as was observed in the EDS analysis.

C. *Electrochemical Measurements*

1. *Polarization curves*

Figures 8(a) and (b) show the open circuit potential E_{ocp} of the coated specimens as a function of the dipping time in a 3 wt pct NaCl solution at room temperature. The experiments were carried out on samples until the data exhibited a fairly constant and reproducible potential (steady state). For the GALVALUME samples, the stability was reached after 600 seconds and the estimated potentials were -998 ± 2, -995 ± 2, -989 ± 2, and -993 ± 1 mV *vs SCE* at 0, 10, 30, and 60 seconds of treatment, respectively (Figure 8(a)). The potentials of chromated coatings are slightly higher than those for the bare samples. The potential difference between the chromated and nonchromated samples varies approximately in 10 mV, and a maximum can be reached after dipping them 30 seconds. On the other hand, the Fe-Zn samples show that the treatment definitively displaced negatively the potential of the samples (Figure 8(b)). After 600 seconds, the potentials of the coatings were -1046 ± 3, -1061 ± 2, -1077 ± 2, and -1065 ± 4 mV *vs SCE* with dipping times of 0, 10, 30, and 60 seconds, respectively. In this case, the potential difference between coated and noncoated samples varies from 15 to 25 mV. By comparing similar dipping times, it was found that GALVALUME showed a more positive displacement in the E_{ocp} than those for the galvanized steel specimens, which is in good agreement with the literature.[38] The obtained values during the OCP measurements indicate that in this electrolyte, the CCCs in both substrates can function as a protective film.[1,2,13–15] Forget and Zhang *et al.*[36,39] have also reported similar potentials for galvanized steel and their chromated coatings have a negative potential with respect to bare zinc. They suggested that the chromate coatings can cathodically inhibit the corrosion of zinc in the solution, and when the anodic reaction remains the same, the corrosion current is reduced and the potential shifts negatively, which could explain the behavior of the Fe-Zn substrates here obtained.

Figure 9 summarizes the *Rp* data. All the treated GALVALUME samples show higher *Rp* values with respect to treated and untreated galvanized steel specimens. However, the galvanized steel treatments resulted in the formation of a more uniform film; their protection barrier broke down faster in contact with the aggressive media. By comparing the behavior of the coatings produced at different immersion times, it is seen that the samples at 30 seconds have the highest *Rp*; *i.e.*, they showed a better corrosion protection. Particularly at this time, a strong difference between GALVALUME and galvanized steel *Rp* values (8595 and 3808 $\Omega\ cm^{-2}$, respectively) was observed.

Figures 10(a) and (b) show the effect of chromating on the polarization behavior of the Fe-Al-Zn and Fe-Zn

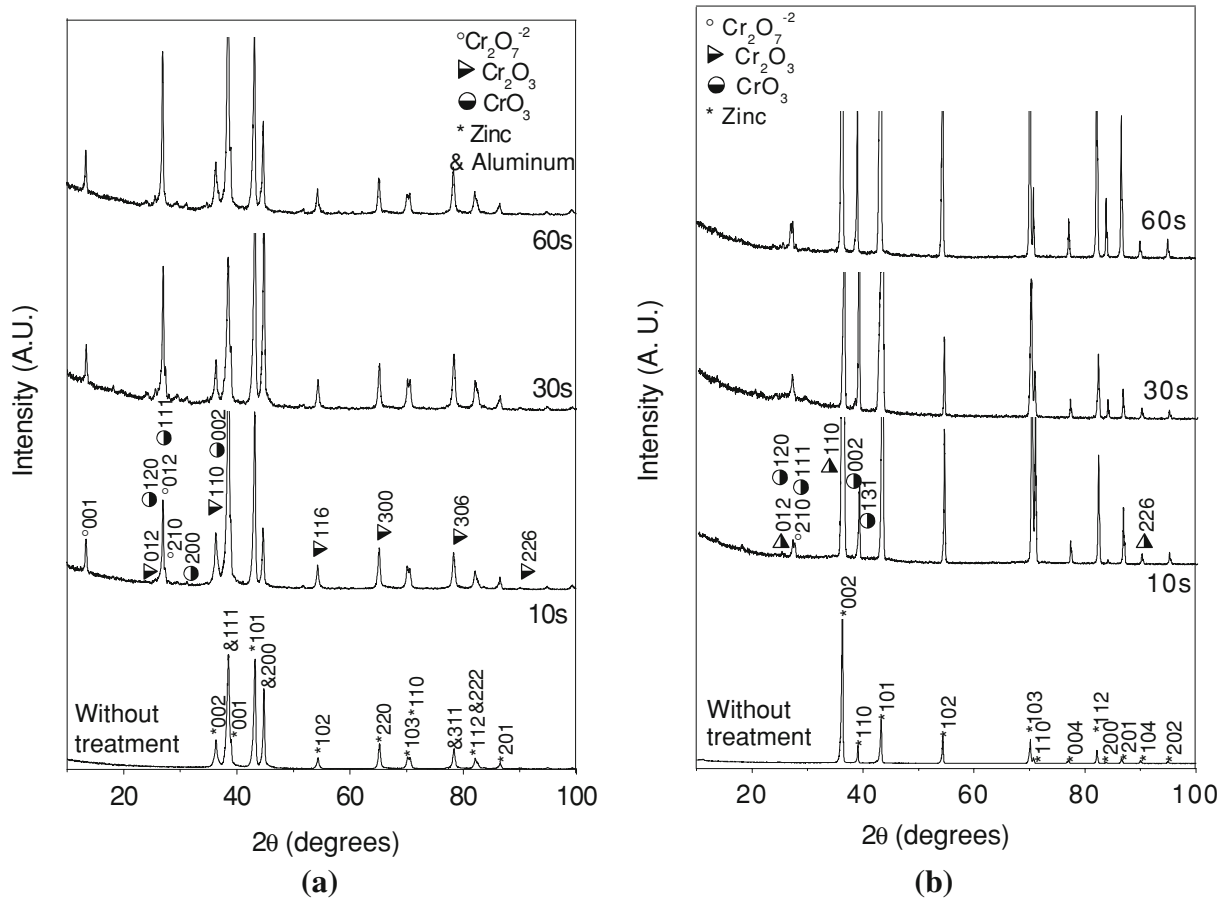

Fig. 7—XRD patterns for treated and untreated specimens: (*a*) GALVALUME and (*b*) galvanized steel.

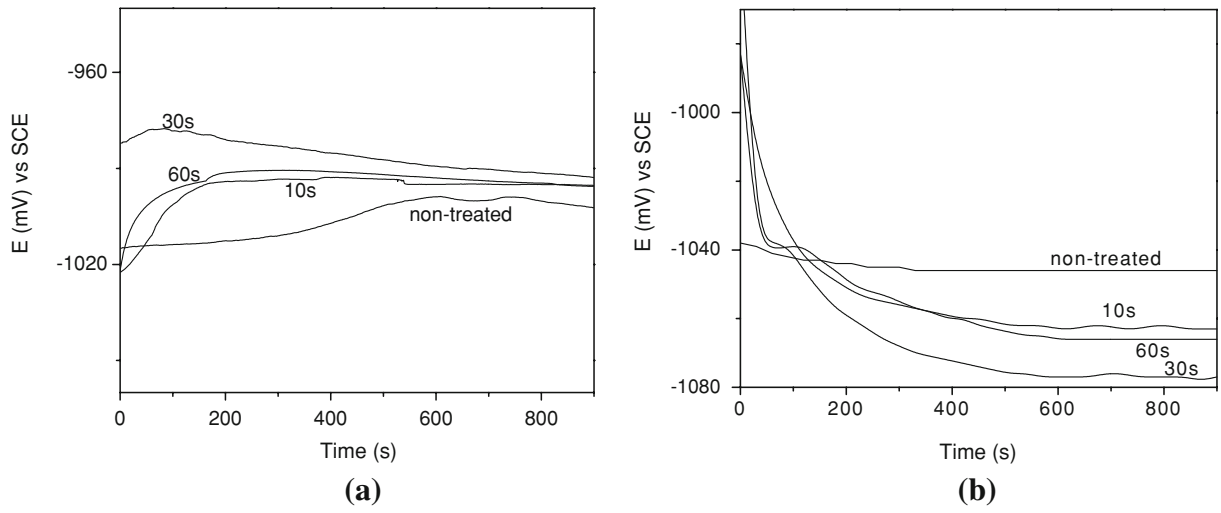

Fig. 8—Open circuit potential *vs* time for (*a*) GALVALUME and (*b*) galvanized steel at 0, 10, 30, and 60 sec of immersion time; pH = 1.1 and room temperature.

substrates. GALVALUME specimens show a quite similar electrochemical behavior concerning the cathodic and anodic polarization curves. However, a displacement can be observed in the corrosion potential when the dipping time is increased (Figure 10(a)). The corrosion potential difference between the chromated GALVALUME and bare GALVALUME samples varies from 30 to 64 mV, respectively. The rest of the

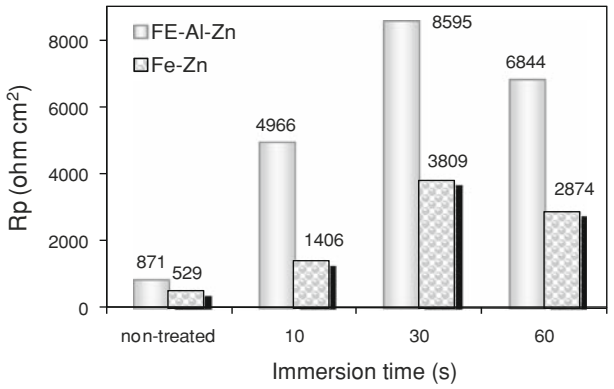

Fig. 9—Polarization resistance values for work electrodes.

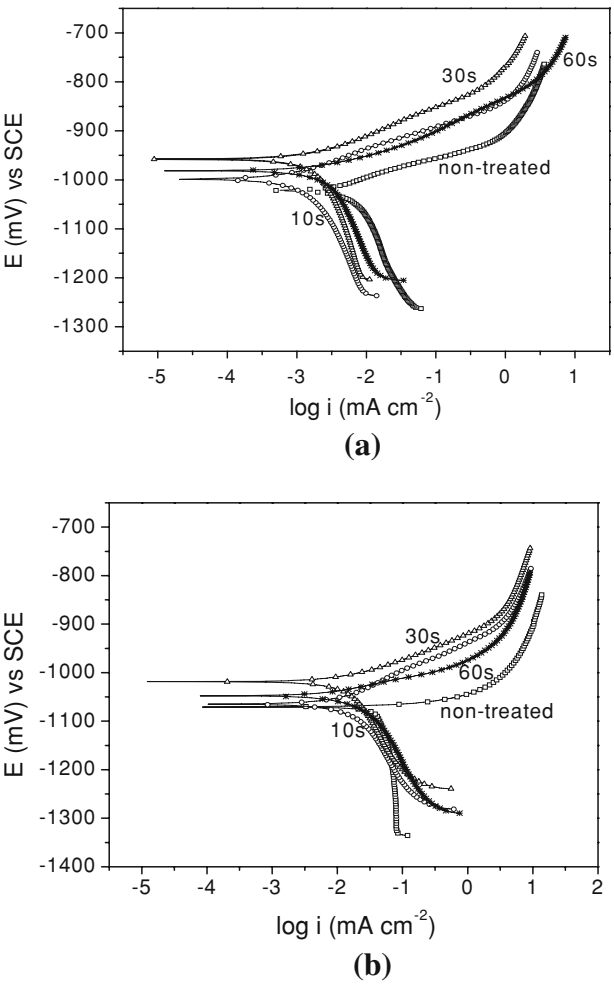

Fig. 10—Tafel polarization curves in a 3 wt pct NaCl aqueous solution: (*a*) GALVALUME and (*b*) galvanized steel specimens.

potentials of galvanized steel were near the rest of the potentials of nonchromated specimens (Table III). The presence of oxichromates on the Fe-Zn surface causes changes in the cathodic slopes. Such changes can be observed as a displacement of the cathodic branch toward lower current densities as well as a slight increase in the corrosion potential of the system. This behavior points to the presence of a porous barrier layer. Additionally, the displayed shift of the anodic curve in the positive direction and the higher current density in this branch shows that the increasing amount of the corrosion products on dark yellow chromated Fe-Zn coating preserves the corrosion protection ability. Recently, Zhang, Turgoose, Nevison, and co-workers[24,40,41] found that zinc corrosion is markedly controlled by oxygen diffusion in a near-neutral aerated solution containing Cl^- anions.[24–26] Additionally, Dafydd *et al.*[42] recently suggested that aluminum is virtually inert and their content in Al-Zn alloys (from 0.1 to 55 pct) exerts little influence on the O_2 reduction kinetics, which may explain the cathodic branch shape obtained for Fe-Al-Zn samples and the relative increase in the cathodic current density of the Fe-Zn substrates after the conversion layers were applied.

The comparison between the polarization curves obtained for GALVALUME and the galvanized steel sheets indicates that the cathodic activities with their corresponding corrosion current densities were largely determined by the substrate properties. The differences observed in the cathodic behavior were dependent on the treatment time (10, 30, and 60 seconds) for both electrodes, which could be attributed to the increase in the adsorption of O^{-2} ions with the amount of chromium on the treated surface.

The values of the corrosion potential (E_{corr}) and the corrosion current density (i_{corr}) for both types of substrates, treated and nontreated, are presented in Table III. In each case, the current density was estimated from a Tafel plot by extrapolating the cathodic and anodic branches. The current densities listed in Table III are the mean current densities on the specimen surfaces; however, the true local density could not be calculated, since the true active reaction area was unknown due to the nonuniformity of the coatings. The current densities for the coated samples are up to 5 times lower than those of the bare samples, but important differences are detected with the dipping time. Specifically, the current densities for the coated sample at 60 seconds (3.09 and 17.78 $\mu A\ cm^{-2}$, for Fe-Al-Zn and Fe-Zn, respectively) are higher than those of the samples with dipping times of 10 and 30 seconds. By increasing the immersion time to 30 seconds, the corrosion resistance increases too; on the other hand, longer conversion times decrease the corrosion resistance. These results can again be explained in terms of tensile stress inside the coating when the chromate layer is growing. Our results are very close to those reported in the literature[43] on the corrosion rates of GALVALUME and galvanized steel, where it has been mentioned that the performance of Fe-Al-Zn is superior *vs* Fe-Zn in all three types of environments (marine, industrial, and rural) with a ratio of average corrosion rates of 4.2, 6.2, and 3.4, respectively.

2. *Electrochemical impedance spectroscopy*

The Nyquist and Bode plots of Fe-Al-Zn and Fe-Zn with different dipping times, in a naturally aerated 3 wt pct NaCl solution, are shown in Figures 11(a)

Table III. Average Corrosion (E_{corr}) and Corrosion Current Density (i_{corr}) Calculated from the Cathodic and Anodic Polarization Curves

	GALVALUME		Galvanized Steel	
Samples	E_{corr} (mV_{SCE})	i_{corr} ($\mu A\ cm^{-2}$)	E_{corr} (mV_{SCE})	i_{corr} ($\mu A\ cm^{-2}$)
Nonchromated	-1020 ± 5	7.41 ± 0.02	-1083 ± 6	46.77 ± 0.5
10 s	-988 ± 8	1.49 ± 0.1	-1058 ± 9	11.75 ± 0.3
30 s	-977 ± 12	1.42 ± 0.3	-1048 ± 8	9.77 ± 0.2
60 s	-956 ± 8	3.09 ± 0.2	-1042 ± 11	17.78 ± 0.4

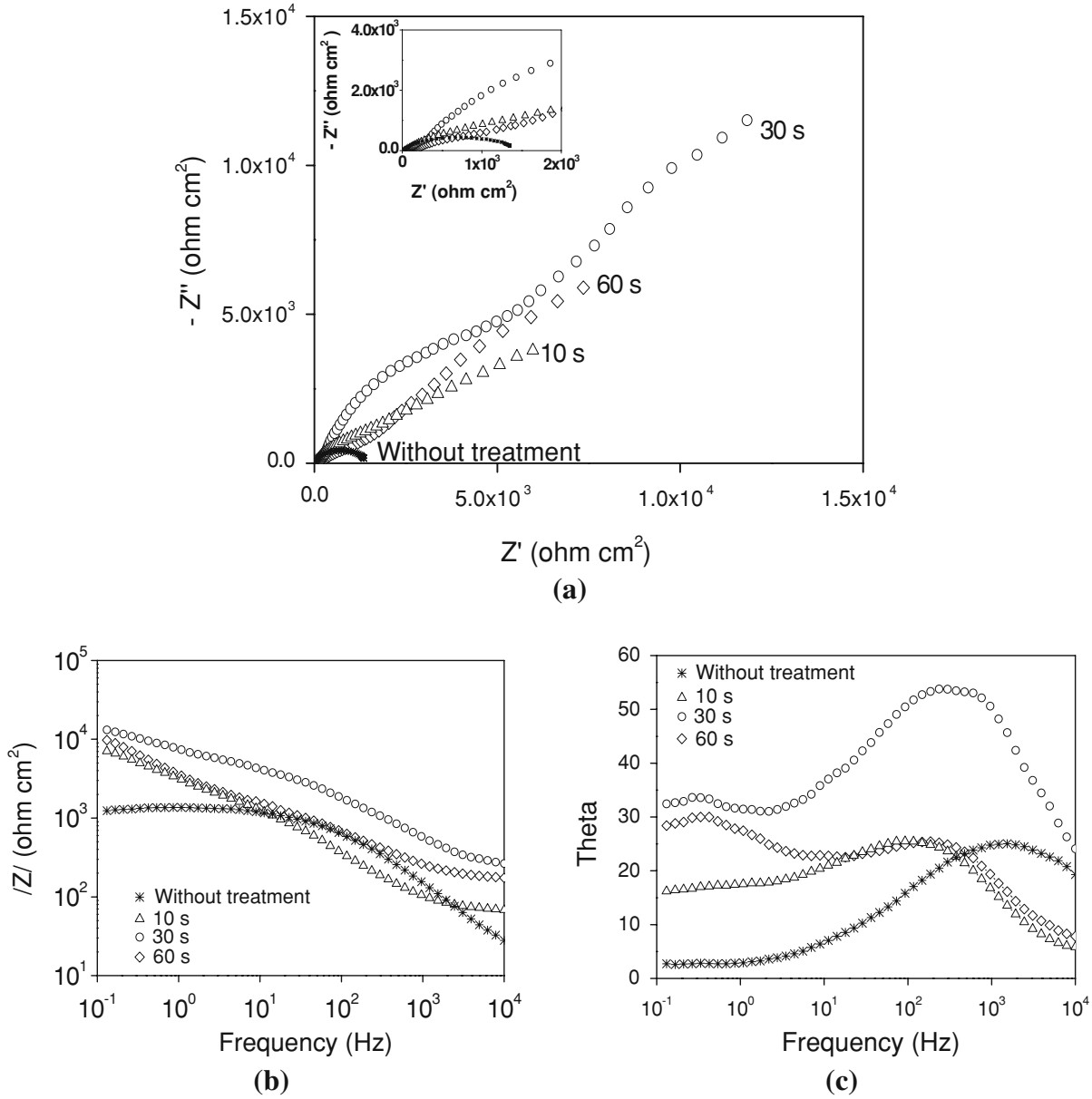

Fig. 11—(*a*) Nyquist and (*b*) and (*c*) Bode impedance plots for GALVALUME for treated and nontreated samples in a 3 wt pct NaCl aqueous solution.

through (c) and 12(a) through (c), respectively. As a reference, the spectra corresponding to an untreated sample are also included. All the diagrams obtained for Fe-Al-Zn sheets show depressed capacitive loops during the sweep at the frequency range. The arc that appears in the Nyquist and Bode plots for the nonchromated samples corresponds to the substrate response. On the other hand, the chromated samples display two

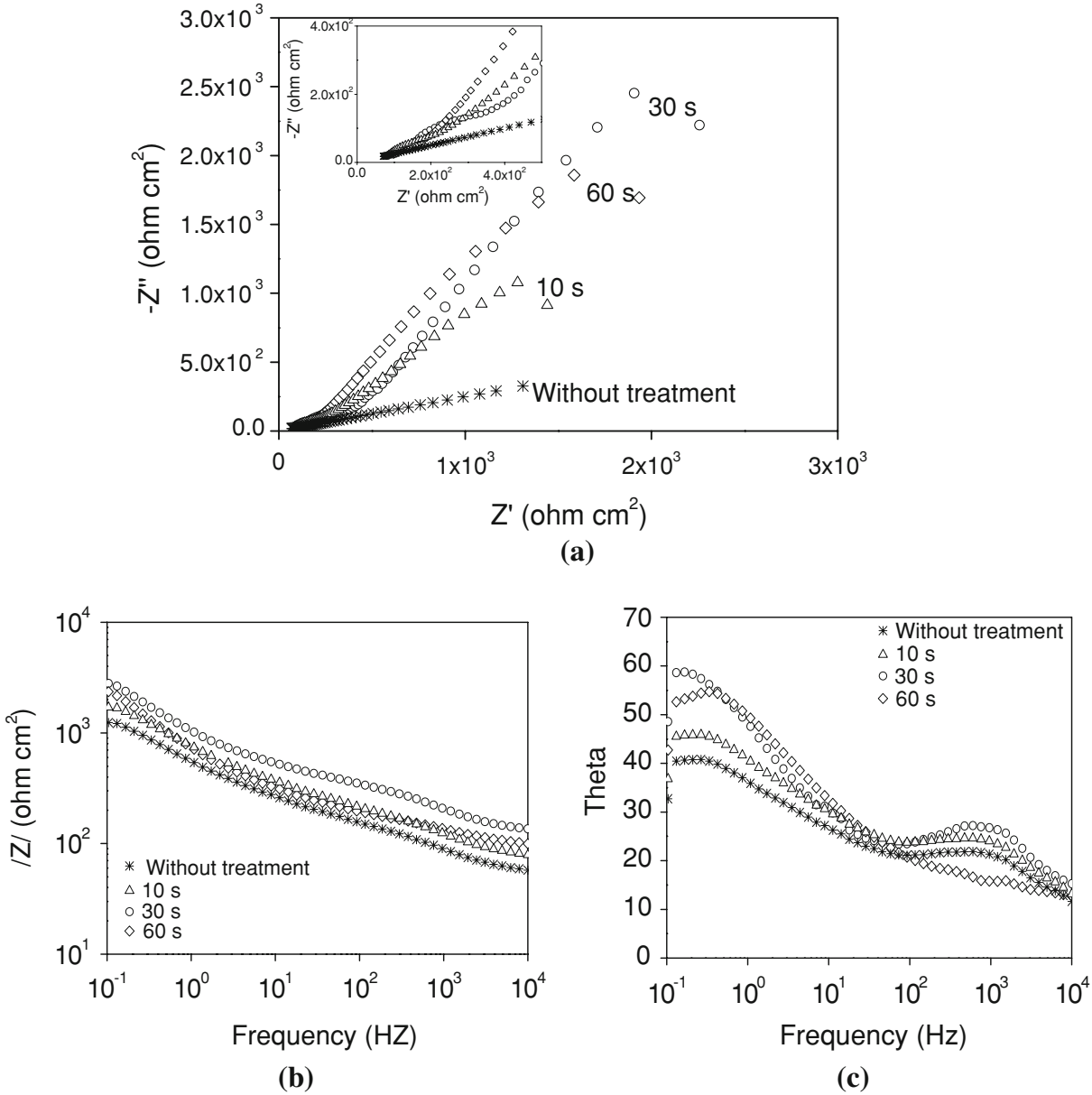

Fig. 12—Nyquist and Bode impedance plots for galvanized steel for treated and nontreated samples in a 3 wt pct NaCl aqueous solution.

capacitive loops. The first semicircle at higher frequencies is due to the protective film (chromating), while the second semicircle at lower frequencies is attributed to the charge transfer process (Figures 11(a) through (c)). The high frequency resistance corresponds to the combination of solution and dissolution or formation of some oxide species during the corrosion process on the surface film. The Bode phase angle diagrams show that an increase in the immersion time up to 30 seconds results in an increase in the phase angle, although a linear trend ($\pi/4$ phase angle) is observed in the high frequency region (inset figure). The coated galvanized steel also shows two semicircles: the first semicircle can be attributed to the chromated layer and the second to the properties of the electric double layer at the interface "galvanized steel-corrosive solution" (Figures 12(a) through (c)).

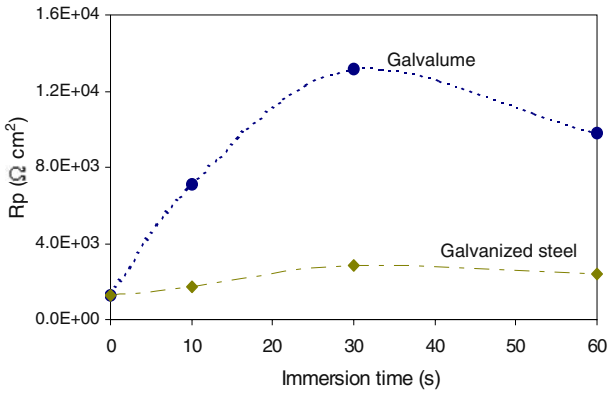

Fig. 13—Resistance polarization of the CCCs in both substrates during EIS measurements.

Table IV. Pull-Off Test Results

	Samples							
	GALVALUME				Galvanized Steel			
Immersion time(s)	0	10	30	60	0	10	30	60
Polyurethane varnish thickness (μm)	86	93	85	94	99	96	87	88
Pressure (lb in.$^{-2}$)	77	104	132	108	60	100	108	108
Detached area (pct)	90	95	85	97	100	90	95	90

In both substrates, when the products of corrosion appear in the cracks and pores of the coating, both semicircles can emerge in one, which is somewhat deformed. The relation of the second semicircle with the corrosive process at the metal surface near the cracks corroborates the significant changes in its diameter with the amount of chromate on the surface and the tensile stress during the growth of the film.

The evolution of the systems during the electrochemical tests is presented in the Bode diagrams (Figures 11 and 12). Two different time constants can be identified in the EIS spectra. Examples of the Bode plots obtained for the Fe-Al-Zn and Fe-Zn samples show that the exposure to the highly aggressive electrolyte (3 wt pct NaCl) causes deterioration of the film. The higher impedance and *Rp* data for the treated samples agree with the results obtained by Tafel, polarization resistance, and SEM observations, and indicate a strong dependence of the chemical conversion treatments on the substrate (Figure 13). By comparing both kinds of samples, it can be observed that GALVALUME offers better anticorrosive properties than the galvanized steel specimens at similar immersion times. This means that although the SEM micrographs show a more uniform film formed on galvanized steel than on the GALVALUME specimens, the chromium–Al-Zn substrate interaction offered a higher anticorrosive performance because of the microstructure of the GALVALUME coating mentioned previously.

D. *Pull-Off Test*

The variation of the adhesive strength of the organic coatings to GALVALUME and the galvanized steel specimens due to the CCCs treatment was evaluated, and the results are shown in Table IV. As can be seen from the table, the average pull-off strength of the polymer varnish to the GALVALUME film without CCCs treatment is about 77 lb in.$^{-2}$, and it was increased to 104, 132, and 108 lb in.$^{-2}$ as the immersion time was increased. Similar results were obtained for the galvanized steel samples, whose adhesion strength was increased from 60 to 100, 108, and 108 lb in.$^{-2}$ for 10, 30, and 60 seconds of treatment, respectively. This indicates that the surface modification by the CCCs improved the adhesion between the substrates and the organic coating. By combining these results with those given by the adherence loss percent, we can also see that the adhesion degree is slightly higher in GALVALUME than in the galvanized steel specimens. This adhesion improvement could be associated with a larger surface roughness for the treated samples or enhanced bonding among the different interfaces.

IV. CONCLUSIONS

The growth of chromate conversion coatings on Fe-Al-Zn and Fe-Zn is highly influenced by both the microstructure and dip-immersion process. The deposited chromium oxide was characterized by a porous morphology and cracks. The crack length per area unit and the size of the crack increase with the dipping times in the chromate bath, which may cause a variation in the surface composition and thickness, favoring the attack of aggressive ions. The conversion coatings grew without preferential direction, since they basically presented the same morphology as the base substrates. The SEM micrographs also show that galvanized steel treatments result in the formation of a more uniform film, but their protection barrier breaks down faster than that of GALVALUME samples in contact with the aggressive media. These results can be explained in terms of both the tensile stress inside the coating when the chromate layer is growing and the dendritic structure of Fe-Al-Zn alloys. The samples that underwent the lowest degree of dissolution were those with a dipping time of 30 seconds. At similar immersion times, the GALVALUME samples have better anticorrosive properties than galvanized steel. This behavior indicates a strong dependence of the chemical conversion treatments on the substrate characteristics, which can inhibit corrosion in this type of solution (NaCl) by hindering the transport of oxygen to the substrate metal. Finally, the CCCs increased the adhesion in both specimens, although it was slightly better in GALVALUME samples.

ACKNOWLEDGMENTS

The authors acknowledge the financial support given by UNAM through the DGAPA PAPIIT IN 115603-project, IPN through SIP-20090561 and 20090499 projects, and SNI-CONACYT through the 61354 project. The authors thank Mr. Ivan Puente L. for the SEM analyses and L. Baños for XRD measurements.

REFERENCES

1. L.F.G. Williams: *Corr. Sci.*, 1973, vol. 13, pp. 865–68.
2. K.A. Korinek: *Metals Handbook*, 9th ed., *Corrosion*, ASM INTERNATIOAL, Metals Park, OH, 1987, vol. 13, pp. 389–95.
3. P.L. Hagans and C.M. Haas: *Surface Engineering*, 10th ed., *ASM Handbook*, ASM INTERNATIOAL, Materials Park, OH, 1994, vol. 5, p. 405.
4. G.D. Wilcox and J.A. Wharton: *J. Trans. IMF*, 1997, vol. 75, pp. B140–42.
5. F.J. Frelin, T.L. Kelly, and A.J. Malloy: U.S. Patent 4,313,769, Amchem Products Inc., India, 1980.
6. L. Fedrizzi, F. Deflorian, S. Rossi, L. Fambri, and P.L. Bonora: *Progr. Organic Coat.*, 2001, vol. 42, pp. 65–74.

7. L. Guangyu, L. Yuan Niu, L. Jianshe, and J. Zhonghao: *Surf. Coat. Technol.*, 2004, vol. 176, pp. 215–21.
8. J.A. Treverton, A. Bosland, and J.M. Brown: *Corr. Sci.*, 1990, vol. 30, pp. 1159–65.
9. F. Mansfeld, S. Lin, S. Kim, and H. Shih: *Electrochim. Acta*, 1989, vol. 34, pp. 1123–32.
10. D.V. Andreva and D.G. Shchukin: *Mater. Today*, 2008, vol. 11, pp. 24–30.
11. F.W. Eppensteiner and M.R. Jenkins: *Met. Finish.*, 2002, vol. 100, Suppl., pp. 179–491.
12. G. Lu, E. Ada, and G. Zangari: *Electrochim. Acta*, 2004, vol. 49, pp. 1461–73.
13. H. Kendig and S. Jean Jaquet: *J. Electrochem. Soc.*, 2002, vol. 149, pp. B47–B51.
14. G.O. Ilevbare and J.R.J. Scully: *J. Electrochem. Soc.*, 2000, vol. 148, pp. B196–B207.
15. P. Campestrini, G. Goeminne, H. Terryn, J. Verecken, and J.H.W. De Wit: *J. Electrochem. Soc.*, 2004, vol. 151, pp. B59–B70.
16. G.M. Brown, K. Shimizu, K. Kobayashi, G.E. Thompson, and G.C. Wood: *Corr. Sci.*, 1993, vol. 34, pp. 1045–54.
17. J.A. Treverton and M.P. Amor: *Appl. Surf. Sci.*, 1986, vol. 25, pp. 183–94.
18. J.A. Treverton and N.C. Davies: *Electrochim. Acta*, 1980, vol. 25, pp. 1571–76.
19. G. Goeminne, C. Wagemans, J. Wagemans, O. Serot, M. Loiselet, and M. Gaelens: *Nucl. Phys. A*, 2000, vol. 678, pp. 11–23.
20. P. Campestrini, S. Böhm, T. Schram, H. Terryn, and J.H.W. De Wit: *Thin Solid Films*, 2002, vol. 410, pp. 76–85.
21. E.J. Wilhelm: U.S. Patent. 2,035,380, New Jersey Zinc Co., 1936.
22. D.A. Jones: *Principles and Prevention of Corrosion*, MacMillan Publishing Company, New York, NY, 1992, pp. 457–70.
23. H.H. Uhlig: *The Corrosion Handbook*, 2nd ed., John Wiley & Sons, Inc., New York, NY, 2000, pp. 1169–78.
24. S. Guessasma, O. Elkedim, P. Nardin, R. Hamzaoui, and T. Grosdidier: *Corr. Sci.*, 2007, vol. 49, pp. 2880–2904.
25. X.G. Zhang: *Corrosion and Electrochemistry of Zinc*, Plenum Press, New York, NY, 1996.
26. A.M. Rocco, T.M.C. Nogueira, R.A. Simao, and W.C. Lima: *Surf. Coat. Technol.*, 2004, vol. 179, pp. 135–44.
27. H.J. Cleary: *16th Annual Technical Meeting of the International Metallographic Society*, Alberta, Canada, July 1983.
28. A. Pfennig and B. Fedelich: *Corr. Sci.*, 2008, vol. 50, pp. 2484–92.
29. H. Asgari, M.R. Toroghinejad, and M.A. Golozar: *Appl. Surf. Sci.*, 2007, vol. 253, pp. 6769–77.
30. J.C. Scully: *The Fundamentals of Corrosion*, Pergamon Press, Oxford, NY, 1990.
31. S. Chang and J.C. Shin: *Corr. Sci.*, 1994, vol. 8, pp. 1425–36.
32. Z.L. Long, Y.C. Zhou, and L. Xiao: *Appl. Surf. Sci.*, 2003, vol. 218, pp. 123–36.
33. O. Lunder, J.C. Walmsley, P. Mack, and K. Nisacioglu: *Corr. Sci.*, 2005, vol. 47, pp. 1604–24.
34. N.M. Martyak, J.E. McCaskie, and L. Harrision: *Met. Finish.*, 1996, vol. 94, pp. 65–67.
35. N.M. Martyak: *Surf. Coat. Technol.*, 1997, vol. 88, pp. 139–46.
36. X. Zhang, W.G. Sloof, A. Hovestad, E.P.M. Van Westing, H. Terryn, and J.H.W. De Wit: *Surf. Coat. Technol.*, 2005, vol. 197, pp. 168–76.
37. T. Schram, J. De Laet, and H. Terryn: *Thin Solid Films*, 1998, vol. 727, pp. 313–17.
38. A.P. Yadav, H. Katayama, K. Noda, H. Masuda, A. Nishikata, and T. Tsuru: *Corr. Sci.*, 2007, vol. 49, pp. 3716–31.
39. L. Forget, J. Delhalle, and Z. Mekhalif: *Mater. Corros.*, 2001, vol. 52, pp. 181–84.
40. S. Turgoose: *Chemical Inhibitors for Corrosion Control*, The Royal Society of Chemistry, Manchester, UK, 1990.
41. D.C.H. Nevison: *Corrosion*, 9th ed., *Metals Handbook*, ASM INTERNATIONAL, Metals Park, OH, 1987, vol. 13, p. 755.
42. H. Dafydd, D.A. Worsley, and H.N. McMurray: *Corr. Sci.*, 2005, vol. 47, pp. 3006–18.
43. L. Sziraki, A. Cziraki, Z. Vertesy, L. Kiss, V. Ivanova, G. Raichevski, S. Vitkova, and Ts. Marinova: *J. Appl. Electrochem.*, 1999, vol. 29, pp. 927–37.